Measurements of CO2, its stable isotopes, O2/N2, and 222Rn at Bern, Switzerland

P. Sturm, M. Leuenberger, F. L. Valentino, B. Lehmann, B. Ihly

Atmos. Chem. Phys. Discuss., 5, 8473–8506, 2005
www.atmos-chem-phys.org/acpd/5/8473/
SRef-ID: 1680-7375/acpd/2005-5-8473
European Geosciences Union

Atmospheric Chemistry and Physics Discussions

Measurements of CO_2, its stable isotopes, O_2/N_2, and ^{222}Rn at Bern, Switzerland

P. Sturm, M. Leuenberger, F. L. Valentino, B. Lehmann, and B. Ihly

Climate and Environmental Physics, Physics Institute, University of Bern, Bern, Switzerland

Received: 20 May 2005 – Accepted: 1 July 2005 – Published: 9 September 2005

Correspondence to: M. Leuenberger (leuenberger@climate.unibe.ch)

Abstract

A one-year time series of continuous atmospheric CO_2 measurements from Bern, Switzerland is presented. O_2/N_2 and Ar/N_2 ratios as well as stable carbon and oxygen isotopes of CO_2 and $\delta^{29}N_2$, $\delta^{34}O_2$ and $\delta^{36}Ar$ were measured periodically in a continuous way during a one year period. Additionally, the ^{222}Rn activity was measured during three months in the winter 2004. Using the correlation from short term fluctuations of CO_2 and ^{222}Rn we estimated a mean CO_2 flux density between February 2004 and April 2004 in the region of Bern of $95\pm39\,tC\,km^{-2}\,month^{-1}$. The continuous observations of carbon dioxide and associated tracers shed light on diurnal and seasonal patterns of the carbon cycle in an urban atmosphere. There is considerable variance in nighttime $\delta^{13}C$ and $\delta^{18}O$ of source CO_2 throughout the year, however, with generally lower values in winter compared to summertime. The O_2:CO_2 oxidation ratio during the nighttime build-up of CO_2 varies between -0.96 and $-1.69\,mol\,O_2/mol\,CO_2$. Furthermore, Ar/N_2 measurements showed that artifacts like thermal fractionation at the air intake are relevant for high precision measurements of atmospheric O_2.

1. Introduction

We present continuous records of atmospheric CO_2 and associated tracers measured in the city of Bern, Switzerland. At this urban site, anthropogenic CO_2 emissions (e.g., car exhausts, heating) mix with the background and biogenic CO_2 components, which are influenced by circulation, photosynthesis and respiration. Local sources and sinks in the catchment area of Bern and changing meteorological conditions are expected to lead to large short-term variations of the observed tracers. In order to be able to interpret and apportion these observations high-resolution measurements of multiple tracers are needed.

Stable carbon and oxygen isotopes in atmospheric CO_2 can be used to measure the size of the CO_2 fluxes and to discriminate between the various processes in the carbon

cycle. Photosynthetic uptake of CO_2, plant and soil respiration, and fossil fuel burning lead to carbon and oxygen isotope signals of atmospheric CO_2, which can be used as a tracer at various temporal and spatial scales (Friedli et al., 1987; Keeling et al., 1989; Ciais et al., 1997a). Hesterberg (1990) has measured $\delta^{13}C$ and $\delta^{18}O$ of CO_2 in Bern during a one-year period in 1988/89. His measurements of flask samples collected twice a week showed seasonal differences in the $\delta^{13}C$ and $\delta^{18}O$ signals (Fig. 1).

Another approach involves measuring changes of the atmospheric oxygen (O_2) concentration. O_2 and CO_2 are inversely coupled by photosynthesis, respiration and combustion. However, the different processes have different O_2:CO_2 exchange ratios and thus can be distinguished from each other. The high precision of O_2 measurements that is necessary to constrain such carbon fluxes, has given new insights into gas handling procedures and fractionation effects (Bender et al., 1994; Keeling et al., 1998; Langenfelds, 2002). Though continuous on-line measurements circumvent any storage related effects as observed in some flask sampling programs (Sturm et al., 2004), they are still susceptible to diffusive fractionation processes. Fractionation of O_2/N_2 at the intake as well as at tees have first been observed by Manning (2001) and have been attributed to molecular thermal diffusion. Yet, the exact cause of the fractionation and the points at which it can occur in the flow path of air are still not well established. Molecular thermal diffusion results from temperature gradients. Heavier molecules generally accumulate in the colder region hence leading to concentration changes (Severinghaus et al., 1996; Chapman and Cowling, 1970).

Radon-222 is a radioactive noble gas with a half-life $T_{1/2}$ of 3.82 days. It is produced in all soils as part of the natural uranium-radium α-decay series and it emanates into the soil air and diffuses to the atmosphere where it is diluted by atmospheric transport and radioactive decay. The ^{222}Rn flux from ocean surfaces is about two orders of magnitude smaller than from continents (Wilkening and Clements, 1975). Because ^{222}Rn emissions from soils turned out to be rather homogeneous in a restricted region and relatively constant in time, ^{222}Rn is a useful tracer to parameterize transport and dilution in the atmospheric boundary layer.

This paper first summarizes sampling and analysis techniques and reports on tests we have performed to assess fractionation effects at the air intake. Results for CO_2, its stable isotopes, O_2/N_2 and ^{222}Rn over roughly a one-year period are described and possible mechanisms for these observations are discussed.

2. Sampling and analysis techniques

2.1. Sampling site

The city of Bern (about 127 000 inhabitants) is situated on the Swiss Plateau. The measurements were made at the Physics Institute, University of Bern (PIUB), which is located on the eastern edge and about 20 m above the city center. The building is surrounded by residential and urban areas. The air is collected from the roof of the building (46°57′04″ N, 7°26′20″ E, 575 m a.s.l.) about 15 m above local ground. Meteorological measurements were made by the Institute for Applied Physics, University of Bern. The weather station is located at the same height about 10 m away from the air intake. The sample air is sucked through a ∼40 m long 6 mm outer diameter Dekabon tube into our laboratory. We use a diaphragm pump (KNF Neuberger, Switzerland, N86KNDC with EPDM diaphragm). The flow rate is between 100 and 300 mL min^{-1} depending on which instruments are connected to the air stream. The air is dried cryogenically at −70°C. The total volume of the cold trap (about 250 mL) restricts the time resolution of the measurements to about 2 min.

2.2. CO_2 mixing ratio

The CO_2 mixing ratio was measured by non-dispersive infrared adsorption (NDIR) technique. In the beginning the CO_2 measurements were performed by a S710 UNOR CO_2 analyzer (SICK MAIHACK GmbH, Germany). From March 2004 a LI-7000 CO_2/H_2O analyzer (LI-COR, USA), was used. The flow rate of the sample gas

ACPD
5, 8473–8506, 2005

is about 100 mL min^{-1} and every minute the mean CO_2 mixing ratio is recorded. The CO_2 data are reported on the WMO CO_2 mole fraction scale. Primary standards from NOAA/CCGG, Boulder, CO, USA, are used to calibrate the working and secondary standards. However, the CO_2 mixing ratio of these primary standards lies in the range of 192 to 363 ppm. The calibration of our CO_2 scale above 363 ppm is therefore based on extrapolation. Still, the accuracy of the CO_2 data is estimated to be better than ±0.5 ppm for mixing ratios below 400 ppm and better than ±1 ppm for 400 to 450 ppm.

2.3. $\delta^{13}C$ and $\delta^{18}O$ of CO_2

The carbon and oxygen isotopes of CO_2 were determined by a combined Gas Chromatography Mass Spectrometric technology (GC/MS) in a semi-continuous way. Every 12 min an air parcel of about 0.5 mL STP was cryogenically trapped in a glass capillary. The small air amount is then released into a low helium stream (1 mL min^{-1}). This gas stream is additionally split into three similar fluxes entering capillaries of different lengths. A multi-port valve handles the flow path such that the three gas portions are injected one after another via an open split device to an isotope ratio mass spectrometer (DELTA^{plus}XL, Thermo Electron, Bremen, Germany), where the m/z ratios 45/44 and 46/44 of the CO_2 are measured (Leuenberger et al., 2003). The precision of this method estimated by the pooled standard deviations of the triplicate measurements is about ±0.08‰ for $\delta^{13}C$ and P±0.12‰ for $\delta^{18}O$. Constant N_2O corrections of −0.23‰ and −0.35‰ are applied to the $\delta^{13}C$ and $\delta^{18}O$ data, respectively. Variations in the N_2O/CO_2 concentration ratio of the sample air would lead to varying N_2O corrections, but such effects are expected to be small compared to the measurement precision. Carbon and oxygen isotopic compositions are expressed on VPDB-CO_2 scale.

$\delta^{18}O$ measurements from flask sampling often face additional experimental problems, due to the risk of isotopic exchange of CO_2 with water, that may occur anywhere in the sample treatment from the moment of sampling until the input of the sample in

the mass spectrometer (Gemery et al., 1996). For example, isotope exchange during flask storage of CO_2 with water, that permeates through the flask seals (Sturm et al., 2004), interferes with any real atmospheric signal. Our flask measurements of $\delta^{18}O$ from Jungfraujoch, Puy de Dôme and Griffin (Sturm et al., 2005b,a) are therefore believed not to represent the true isotopic composition of atmospheric CO_2. Therefore the advantage of the continuous analysis method used here, apart from the high time resolution, is that such storage related effects can largely be circumvent.

2.4. Elemental and isotopic ratios of air

The elemental ratios O_2/N_2 and $\delta Ar/N_2$ as well as the isotopic ratios $\delta^{29}N_2$, $\delta^{34}O_2$ and $\delta^{36}Ar$ are analyzed by an isotope ratio mass spectrometer (DELTA^{plus}XP, Thermo Electron, Bremen, Germany) and expressed in the δ-notation as per meg deviation from our local PIUB reference gas. A glass capillary at a tee takes about 0.2 mL min^{-1} of the flow to the gas inlet system (Leuenberger et al., 2000; Sturm, 2001) of the IRMS. One measurement comprises eight standard/sample cycles and takes about 12 min. Hence one data point represents a mean concentration of the last 12 min.

2.5. ^{222}Rn activity

The specific ^{222}Rn activity is measured by an alpha-decay detector (Alphaguard 2000 Pro, Genitron Instruments, Frankfurt, Germany). The instrument was placed on the roof of the PIUB building, about 10 m next to the air intake. Using digital signal processing for pulse shape analysis the detection limit of the detector in a 10 min measuring interval is about 3 Bq m^{-3} (Lehmann et al., 2004).

3. Results and discussion

3.1. Temperature dependent fractionation at the air intake

The Ar/N_2 ratio can be measured simultaneously with O_2/N_2 and is a useful tracer to reveal fractionation effects. Only the temperature dependence of the gas solubility in seawater leads to seasonal variations in air-sea fluxes and small changes in atmospheric Ar/N_2 ratio (Keeling et al., 2004). On diurnal timescales, however, the atmospheric Ar/N_2 ratio is expected to be constant, because no biogeochemical processes influence these inert gases. However, our Ar/N_2 measurements revealed large variability. Diurnal variations of $\delta Ar/N_2$ and outdoor temperature are shown as an example in Fig. 2. The outdoor temperature was measured by a HOBO H8 data logger (Onset Computer Corporation, MA, USA) placed at the bottom of the intake pole. The air intake is a Dekabon tube with 4 mm inner diameter (ID) and the flow rate was about 250 mL min^{-1}. The higher the air temperature is, the lower the $\delta Ar/N_2$ gets.

To assess the causes of the observed $\delta Ar/N_2$ variations and to better quantify this effect, we conducted tests with different intake tubes and sampling flows. In addition to the Dekabon tube with flow rates of 250 mL min^{-1} and 35 mL min^{-1}, also a stainless steel tube with 0.8 mm ID and a flow rate of 155 mL min^{-1} was used. The correlation of $\delta Ar/N_2$ and outdoor temperature for different types of air intakes is shown in Fig. 3. Remarkably, the temperature records lag the $\delta Ar/N_2$ variations by 90 to 150 min. This is probably due to a slow response of the temperature logger used for these tests and the fact that the temperature sensor was not exposed to sunlight in contrast to the air intake. This time shift was applied in the calculations of Fig. 3 to obtain the best correlation. The temperature sensitivities obtained by geometric mean regression are -17.5 ± 0.6 per meg/°C (R^2=0.70), -7.2 ± 0.2 per meg/°C (R^2=0.71) and -3.6 ± 0.2 per meg/°C (R^2=0.51) for the "4 mm ID/35 mL min^{-1}", "4 mm ID/250 mL min^{-1}" and "0.8 mm ID/155 mL min^{-1}" experiments, respectively. As shown in Fig. 4, the temperature sensitivities of $\delta Ar/N_2$ mainly depend on the gas velocity at the air intake.

Variations of the laboratory temperature can also potentially influence the $\delta Ar/N_2$ measurements. Especially in summer there is a diurnal cycle of the laboratory temperature with amplitudes of 2 to 3°C. However, the most striking feature of the diurnal temperature variations in the laboratory is a rapid drop of about 3°C at midnight caused by the air-conditioning. Because in these experiments no change in $\delta Ar/N_2$ can be observed at midnight, the variations in $\delta Ar/N_2$ are indeed mainly caused by fractionation at the air intake. This supposition was further confirmed by actively heating the intake tube, which resulted in large $\delta Ar/N_2$ deviations. An explanation is that during the day especially when the sun heats the black coating of the Dekabon tube, there builds up a small temperature gradient between the intake tube and the surrounding air. This leads to thermal diffusion with preferential accumulation of the lighter molecules in regions with higher temperatures. A thermal diffusion factor for Ar in N_2 of α=0.071 (Grew and Ibbs, 1952) would lead to a steady state fractionation of 240 per meg/°C. However, a steady state is not achieved at the intake because of the continuous flow of gas. Even though, the lower the flow velocity the more the air can approach a steady state. The slope of the correlation plot of $\delta Ar/N_2$ versus O_2/N_2 for the "4 mm ID/35 mL min^{-1}" and the intake heating experiments gives 3.8±0.1 (Fig. 5a) and is in good accordance with what is expected from thermal fractionation (Grew and Ibbs, 1952; Keeling et al., 2004).

The isotopic ratios $\delta^{29}N_2$, $\delta^{34}O_2$ and $\delta^{36}Ar$ show also small variations that are correlated with the temperature, providing compelling evidence of diffusive fractionation. However the signal-to-noise ratio relative to measurement precision is much higher for Ar/N_2 than for $\delta^{29}N_2$, $\delta^{34}O_2$ or $\delta^{36}Ar$, because Ar/N_2 is more sensitive to mass-dependent fractionation processes owing to the comparatively large mass difference between Ar and N_2. Figure 5b, c and d show the correlation plots of $\delta Ar/N_2$ versus $\delta^{29}N_2$, $\delta^{34}O_2$ and $\delta^{36}Ar$ for the "4 mm ID/35 mL min^{-1}" experiment. The mass spectrometric uncertainty is indicated by error bars in the lower right corner of each plot. Regression lines (black lines) were calculated in Fig. 5a, b and c using a measurement error model which accounts for the relative magnitude of the errors in both variables

(Fuller, 1987). There is no correlation between $\delta Ar/N_2$ and $\delta^{36}Ar$ (Fig. 5d). The thermal diffusion factors α of $^{29}N_2$-$^{28}N_2$, $^{34}O_2$-$^{32}O_2$ and ^{36}Ar-^{40}Ar at 20°C are about 0.0045, 0.0099 and −0.0137, respectively (Lang, 1999). The expected correlation slopes for thermal diffusion obtained from these diffusion factors are shown as grey lines in Fig. 5. Measurements of the isotopic composition of N_2, O_2 and Ar are further discussed in Sect. 3.4.

Experiments showed that the thermal fractionation at the intake could be reduced if instead of Dekabon other types of tubing are used. Intakes both made of transparent plastic and stainless steel significantly reduced this effect, presumably because of a smaller influence of solar heating. However, thermal fractionation could also be observed on days with overcast sky. Shading of the intake from sunlight can therefore only reduce but not eliminate this effect. High flow velocities at the intake either by large sampling flows or by intake tubes with small inner diameters may be most helpful for reducing thermal diffusion at the intake.

Additional tests with sample air from a high pressure cylinder showed that there is also a measurable influence of the laboratory temperature on $\delta Ar/N_2$. A cylinder was placed outside the laboratory where only small and not abrupt temperature variations occur to exclude any fractionation related to the cylinder or the pressure regulator. Then, the measured $\delta Ar/N_2$ showed to be positively correlated with the laboratory temperature (in contrast to the negative temperature sensitivity for fractionation at the intake). Different sources of thermal fractionation inside the laboratory may lead to these effects: a) The cold trap which is partly immersed in silicon oil at −70°C. Because of the relatively large volume (~250 mL) and the large temperature gradient (~90°C) thermal diffusion is likely to occur inside this cold trap. Changing temperature gradients due to varying room temperatures could therefore lead to thermal effects. b) Temperature dependent fractionation at tees (Manning, 2001), and c) Fluctuations of the working gas due to thermally induced effects at the high-pressure gas cylinders. We favor explanation b) based on first tests of divided air fluxes by tees showing a clear thermal diffusion effect.

3.2. The CO_2 record

The prevalent local wind directions are the northern and western wind sector. High wind speeds occur with winds coming from north-east to east (45 to 90°) and from west to south-west (225 to 270°), which are the predominant mesoscale wind directions on the Swiss Plateau. Generally, there is a good correlation between CO_2 and ^{222}Rn for all wind directions. Also, no significant correlation between wind direction and CO_2 mixing ratio was found, indicating that no distinct CO_2 sources are in the immediate vicinity of the sampling site.

An overview of atmospheric records of CO_2, ^{222}Rn, O_2/N_2, $\delta^{13}C$ and $\delta^{18}O$ of CO_2 at Bern between October 2003 and February 2005 is given in Fig. 6. The diurnal variability is much larger than the seasonal variability and is mainly caused by local sources and sinks and by diurnal changes of atmospheric mixing conditions in the boundary layer.

CO_2 mixing ratios were highest in the wintertime with nighttime maximum values reaching more than 500 ppm. During atmospheric inversion events, characterized by persistent fog in autumn and winter, the CO_2 mixing ratio was clearly above 400 ppm over a period of several days. Afternoon values in the spring and summer were commonly close to the background value as measured for example at Jungfraujoch (Sturm et al., 2005b). Figure 7 shows the monthly mean diurnal amplitudes and the monthly mean of the CO_2 mixing ratio for the months October 2003 to February 2005. Diurnal variations of CO_2 show a minimum in the afternoon followed by an increase towards the maximum in the early morning hours. The diurnal CO_2 amplitudes are largest in summer (55 to 60 ppm peak-to-peak) and smallest in winter (15 to 25 ppm peak-to-peak) but the monthly amplitudes (i.e. the difference between the monthly maximum and the monthly minimum) are smallest in summer (118 to 128 ppm peak-to-peak) and largest in winter (120 to 148 ppm peak-to-peak) due to inversion events as mentioned above.

The ^{222}Rn activity was measured during a three month period between 27 January and 26 April 2004. The specific activity ranged from 0 to 20 $Bq\,m^{-3}$. Elemental ratios

(O_2/N_2, Ar/N_2) and carbon and oxygen isotopes of CO_2 ($\delta^{13}C$, $\delta^{18}O$) could only be measured periodically, especially on weekends when no other applications and measurements were running on the analyzers. The O_2/N_2, $\delta^{13}C$ and $\delta^{18}O$ showed also large diurnal variations corresponding to changes in CO_2 mixing ratio.

3.3. $\delta^{13}C$ of CO_2, $\delta^{18}O$ of CO_2 and O_2/N_2 measurements

Figure 8 shows an example for typical diurnal cycles of CO_2, O_2/N_2, $\delta^{13}C$ and $\delta^{18}O$ records between 26 April and 1 May 2004. The O_2/N_2, $\delta^{13}C$ and $\delta^{18}O$ measurements mirror the CO_2 variations. The influence of thermal fractionation on O_2/N_2 was corrected using the $\delta Ar/N_2$ measurements. In a first step, the biogenic and anthropogenic components of O_2/N_2 variations were removed by subtracting the CO_2 record scaled by the observed O_2:CO_2 ratio. Variations in the residual O_2/N_2 are then expected to represent thermal fractionation effects. Secondly, the fractionation ratio of O_2/N_2 and $\delta Ar/N_2$ was determined by the correlation between the residual O_2/N_2 and $\delta Ar/N_2$. The slope of this correlation varies between 3.9 and 1.7 (R^2=0.8 to 0.4), which either reflects mixed influences of laboratory and outdoor temperature fractionation or different flow conditions in the inlet system depending on the measurement setup or the low signal to noise ratio. With this O_2/N_2-Ar/N_2 fractionation ratio, the $\delta Ar/N_2$ variations are then used to finally subtract the thermally induced O_2/N_2 variations from the original O_2/N_2 to obtain the corrected O_2/N_2. In Fig. 8 the original (shaded line) as well as the corrected O_2/N_2 (black line) are shown. The correction is less than 5% of the measured O_2/N_2 signal.

A representative Keeling plot of $\delta^{13}C$ and $\delta^{18}O$ (Keeling, 1958, 1961) and the corresponding O_2–CO_2 correlation during the night of 27/28 April 2004 is shown in Fig. 9. Only nighttime values (18:00 to 06:00 LT) have been used to match the Keeling plot assumptions, i.e., a constant background CO_2 concentration and a constant isotopic signature of the source or sink, as accurately as possible. Still, the $\delta^{13}C_{source}$, $\delta^{18}O_{source}$ and O_2:CO_2 ratios mostly represent a flux weighted average of more than one source

and/or sink. Varying proportions of CO_2 sources containing distinct isotope ratios violate the assumptions of the 2-ended mixing model, and are more common with oxygen than carbon isotopes, causing poorer relationships between $\delta^{18}O$ and $1/CO_2$. In Fig. 10 the nighttime buildup of CO_2 was used to derive daily values of $\delta^{13}C_{source}$, $\delta^{18}O_{source}$ and O_2:CO_2 by the Keeling plot intercept method. The correlations were calculated by geometric mean regression and error bars are the standard deviation of the slopes. Only nights with more than 25 measurements, correlation coefficients larger than R^2=0.9 for $\delta^{13}C$ and O_2:CO_2 and larger than R^2=0.7 for $\delta^{18}O$ were considered. The nighttime $\delta^{13}C_{source}$ varies between −33‰ and −25‰ with generally lower values in the winter months than during the rest of the year. This likely represents the larger influence of fossil fuel combustion in wintertime. The large variability from one night to the next may be caused by different weather conditions resulting in advection of different air masses or changes in the CO_2 source distribution. A similar picture can be seen for the nighttime $\delta^{18}O_{source}$. The values range from −34‰ to −3‰ with the depleted (more negative) signatures again occurring in wintertime and highly enriched (more positive) values in the spring and summer. This seasonal variation of $\delta^{18}O_{source}$ is somewhat larger than the variations of about −21‰ to −11‰ observed by Pataki et al. (2003) in a similar study. The $\delta^{18}O$ signal of atmospheric CO_2 is a signal dominated by CO_2 exchange with the terrestrial biosphere (Ciais et al., 1997a,b; Keeling, 1995). Fractionation of the oxygen isotopes of CO_2 occurs in plants owing to differential diffusion of $C^{18}O^{16}O$ and $C^{16}O^{16}O$ and to isotope effects in oxygen exchange with chloroplast water. The higher $\delta^{18}O$ values in summer compared to winter are most probably caused by strong photosynthetic activity and an associated exchange of ^{18}O with leaf water in plants, which is generally enriched in $\delta^{18}O$ if compared to the ground water due to evapotranspiration (Dongmann et al., 1974). Furthermore, CO_2 from combustion has a $\delta^{18}O$ value similar to the $\delta^{18}O$ of atmospheric O_2 at −18‰ on the VPDB-CO_2 scale, corresponding to 23.5‰ on the SMOW scale (Kroopnick and Craig, 1972). Thus a larger fossil fuel CO_2 component in winter leads to decreased $\delta^{18}O$ values.

For a possible interpretation of the observed O_2:CO_2 ratios we consider a simple model. If we assume that the diurnal variations can be described by biogenic and fossil fuel fluxes of carbon and oxygen in the catchment area of the sampling site, then the atmospheric mass balance for CO_2 and O_2 can be written

$$\Delta CO_2 = F + B \tag{1}$$

and

$$\Delta O_2 = \alpha_F F + \alpha_B B, \tag{2}$$

where ΔCO_2 and ΔO_2 are the observed changes in the atmospheric CO_2 and O_2 concentration, F and B are the fluxes of carbon to the atmosphere due to fossil fuel combustion and the terrestrial biosphere, respectively (positive for release to the atmosphere). The coefficients α_F and α_B are average O_2:CO_2 exchange ratios for fossil fuel and land biota. We use $\alpha_F = -1.4\,\mathrm{mol\,O_2/mol\,CO_2}$ (Manning, 2001) and $\alpha_B = -1.1\,\mathrm{mol\,O_2/mol\,CO_2}$ (Severinghaus, 1995). By combining Eqs. (1) and (2) and assuming that F and B are constant over the considered time period, we can estimate from the observed O_2:CO_2 exchange ratio ($\Delta O_2/\Delta CO_2$) the proportion of the biogenic flux in relation to the fossil fuel flux

$$\frac{B}{F} = -\frac{\Delta O_2/\Delta CO_2 - \alpha_F}{\Delta O_2/\Delta CO_2 - \alpha_B}. \tag{3}$$

The measured nighttime O_2:CO_2 oxidation ratios from April 2004 to February 2005 are between −0.96 and −1.69 (lowest panel in Fig. 10). For nighttime air sampling it is assumed that respired CO_2 is added to the atmosphere and both fluxes F and B are positive. This would lead to O_2:CO_2 ratios between −1.1 and −1.4. However, almost half of the summer values are between −0.96 and −1.1. This could only be explained with a biogenic CO_2 sink up to four times as strong as the fossil fuel source, which is obviously not the case, since the CO_2 concentration is increasing and not decreasing during the night. The same considerations can also be applied to the $\delta^{13}C_{source}$

data, where no conflicting picture can be seen. The measured $\delta^{13}C_{source}$ are in the range between an assumed $\delta^{13}C$ of the biospheric component of about −26‰ and the more depleted values of the fossil fuel component. One possibility to explain these low O_2:CO_2 ratios would be an overestimation of the span of our CO_2 scale by more than 10%. Comparison of our CO_2 data with CO_2 measurements from Laboratoire des Science du Climat et de l'Environnement, CE Saclay, France, (Sturm et al., 2005a) and our internal measurements of the calibrated NOAA CO_2 standards on the WMO CO_2 scale lead to the conclusion that this is highly unlikely. An underestimation of the O_2/N_2 span of this magnitude can not be ruled out a priori, though. Since international intercomparison programs for O_2/N_2 measurements are being initiated only now, we do not have any independent validation of our O_2/N_2 scale yet. Measurement effects related to the mass spectrometric technique like cross contamination (Meijer et al., 2000) could potentially lead to an underestimation of the O_2/N_2 span. However, no such effects have been reported by other laboratories also measuring O_2/N_2 by mass spectrometry so far. Another alternative to explain the observed O_2:CO_2 ratios is that processes with O_2:CO_2 exchange ratios of about −1.0 play a major role in nighttime build-up of CO_2. Stephens et al. (2001) have also reported on O_2:CO_2 relationships that are considerably lower than theory would suggest, but potential atmospheric or physiological origins for such relationships are unknown.

3.4. $\delta^{29}N_2$, $\delta^{34}O_2$ and δ^{36}Ar of air

Measurements of the isotopic composition of N_2, O_2 and Ar are shown in Fig. 11. These isotopic ratios are as a first approximation constant within measurement precision. The small variations of the mean appearing in Fig. 11 are due to changes in mass spectrometer performance. Owing to the relatively high sampling rate of 5 measurements per hour, there are also diurnal variations detectable. However, because of the many gaps in the available record and the poor signal-to-noise ratio it is difficult to quantify these effects. As already mentioned in Sect. 3.1, thermal diffusion fractionation at

the air intake is considered to be the dominant cause for such diurnal variations. An assumed variation in $\delta Ar/N_2$ of 200 per meg due to thermal diffusion would correspond to variations in $\delta^{29}N_2$, $\delta^{34}O_2$ and $\delta^{36}Ar$ of about 13, 28 and 39 per meg, respectively. This might be consistent with the observed variations in $\delta^{29}N_2$ and $\delta^{34}O_2$. For $\delta^{36}Ar$ the measured amplitude of the variations are estimated to be larger (about 150 per meg), thus $\delta^{36}Ar$ is probably also influenced by other unidentified measurement artifacts.

The $\delta^{18}O$ of atmospheric O_2 ($\delta^{34}O_2$) is affected by photosynthesis and respiration in the carbon/oxygen cycle and by the hydrological cycle, similar to the oxygen isotopic composition of CO_2. Could we potentially detect biogeochemical variations of $\delta^{18}O$ of atmospheric O_2 in our record? The $\delta^{18}O$ of atmospheric oxygen is enriched by 23.5‰ relative to average ocean water (Kroopnick and Craig, 1972), which is known as the Dole effect. The $\delta^{18}O$ produced by photosynthesis is similar to that of the water from which the oxygen isotopes originate, whereas respiration fractionates by about −20‰ relative to atmospheric O_2 (Guy et al., 1993). The $\delta^{18}O$ of leaf water is elevated by 4 to 8‰ compared to oceanic water due to evapotranspiration (Dongmann, 1974; Farquhar et al., 1993). If we assume that a diurnal increase in atmospheric O_2/N_2 of 500 per meg is driven by the input of photosynthetic O_2 that is about 20‰ lower in $\delta^{18}O$ than atmospheric O_2, we would expect a change in $\delta^{18}O$ of O_2 of 10 per meg. The seasonal variability of O_2/N_2 (~150 per meg) leads to an even smaller signal in $\delta^{18}O$ of O_2 (~3 per meg). The measurement precision defined as the standard deviation of a single measurement is about 40 per meg for $\delta^{34}O_2$. Thus, detecting such small variations is very difficult with current mass spectrometric measurements.

3.5. ^{222}Rn tracer method to estimate regional CO_2 emissions

Examples of hourly mean values of CO_2 and ^{222}Rn, together with local wind speed and wind direction between 17 and 23 March 2004 and between 1 and 7 April 2004 are shown in Fig. 12. During the first days of these periods wind speeds are low with frequently changing directions. The trace gas concentration records show a typical

diurnal pattern caused by nighttime inversion situations. On 19 March and 4 April, respectively, winds change to westerly directions with persistently high wind speeds. The CO_2 and ^{222}Rn concentrations are then close to continental background level (Schmidt et al., 1996). The correlation between ^{222}Rn and CO_2 will be used to estimate CO_2 fluxes for the catchment area of the sampling site.

The ^{222}Rn measurements can be used to infer CO_2 emission by using a simple one-dimensional approach. This method has been used for other greenhouse gases and at different sites and is described in detail by Schmidt et al. (2001). Assuming that each trace gas is released to the atmosphere at a constant rate $\bar{j}_i$ and that it accumulates in a well-mixed boundary layer of height $H(t)$, the short-term change in concentration $\Delta c_i(t)$ is then:

$$\frac{\Delta c_i(t)}{\Delta t} = \frac{\bar{j}_i}{H(t)}. \quad (4)$$

Since $H(t)$ is the same for ^{222}Rn and CO_2, we can eliminate $H(t)$ by combining both tracers

$$\bar{j}_{CO_2} = \bar{j}_{Rn} \frac{\Delta c_{CO_2}}{\Delta c_{Rn}}. \quad (5)$$

The CO_2 flux can thus be calculated from the measured slope between CO_2 and ^{222}Rn variations and the ^{222}Rn exhalation rate. The radioactive decay of ^{222}Rn in the atmosphere during a typical nighttime inversion situation lasting about 12 h leads to a net ^{222}Rn loss of about 5%. Therefore a mean correction factor of 0.95 is applied when estimating ^{222}Rn-based CO_2 fluxes.

Daily CO_2/^{222}Rn correlations were determined using geometric mean regression. To derive a mean value for the period from February to April 2004 only those days were included for which more than 12 hourly mean values existed and which showed a correlation coefficient larger than R^2=0.4. 33 days (39%) satisfy this criterion. The

mean $CO_2/^{222}Rn$ slope is 5.2±1.7 ppm/Bq m^{-3}. This is larger than estimates from other European sites. Schmidt et al. (1996) have measured CO_2–^{222}Rn slopes at Schauinsland, Germany, in the range of 1.8 to 3.5 ppm/Bq m^{-3} for the winter months. A wintertime estimation for western Europe from the Mace Head record by Biraud et al. (2000) gives a slope of 1.4 to 2.1 ppm/Bq m^{-3} for all selected events and 4.7 to 6.8 ppm/Bq m^{-3} for "polluted" events.

The ^{222}Rn flux emitted over continents is not strictly uniform, but depends mainly on the soil type and the hydrological conditions. There is no regional map of observed ^{222}Rn emissions available, but ^{222}Rn flux measurement at different sites in Germany showed an average flux of about 50 Bq m^{-2} h^{-1}, corresponding to 0.7 atoms cm^{-2} s^{-1} (Dörr and Münnich, 1990; Schmidt et al., 2001). The uncertainty of the ^{222}Rn exhalation rate is estimated as ±25% (Schmidt et al., 2001). Using this estimation of the ^{222}Rn exhalation rate one obtains a mean CO_2 flux density during the period February/March/April 2004 for the Bern region of 11.0±4.5 mmole m^{-2} h^{-1} or 95±39 tC km^{-2} month^{-1}. This CO_2 flux includes both biogenic and fossil fuel fluxes. The two main sources of uncertainty for this estimate, namely the ^{222}Rn flux and the $CO_2/^{222}Rn$ correlation amount to an overall uncertainty of the CO_2 flux estimate of ±41%. To reduce this uncertainty the exact source areas of both CO_2 and ^{222}Rn should be known. This would require a explicit transport model, which can resolve the spacial and temporal patterns of the CO_2 and ^{222}Rn sources.

4. Summary and outlook

We summarize first results from on-going continuous measurements of CO_2, its stable isotopes and O_2/N_2 in Bern. Concurrent Ar/N_2 measurements revealed that diffusive fractionation due to thermal gradients at the air intake is an important modifying process for high precision O_2/N_2 measurements. The CO_2, O_2/N_2, $\delta^{13}C$ and $\delta^{18}O$ of CO_2 data show strong diurnal and seasonal cycles. The diurnal variations are modu-

lated by surface uptake and release by vegetation and soils, emissions from fossil fuel combustion, and by the diurnal development of the atmospheric boundary layer. Both stable carbon and oxygen isotopes showed depletion in the winter and enrichment in the summer due to changes in the proportions of fossil fuel combustion and biogenic respiration at different times of the year. Additionally, ^{222}Rn was used to estimate a mean CO_2 flux density in the catchment area of the sampling site. As the measurements go on and more data are available the CO_2 isotope and mixing ratio data can be used to quantify with a mass balance calculation the proportional contribution of each component to the total CO_2 source. We also expect to observe inter-annual variations of the seasonal cycle, and changes in CO_2 mixing ratio relative to background sites, such as Jungfraujoch. Comparison of boundary layer mixing ratios with background mixing ratios should help to improve our understanding of atmosphere/surface exchange of CO_2 on the continental scale.

Acknowledgements. We thank P. Nyfeler for technical assistance, L. Martin (Institute of Applied Physics, University of Bern, Switzerland) for providing the meteorological data and R. Hesterberg for the δ^{13}C and δ^{18}O data of Fig. 1. This work was supported by the Swiss National Science Foundation, in particular the R'equip program, and the EU Projects AEROCARB and CARBOEUROPE-IP.

References

Bender, M. L., Tans, P. P., Ellis, T. J., Orchardo, J., and Habfast, K.: A high precision isotope ratio mass spectrometry method for measuring the O_2/N_2 ratio of air, Geochim. Cosmochim. Acta, 58, 4751–4758, 1994. 8475

Biraud, S., Ciais, P., Ramonet, M., Simmonds, P., Kazan, V., Monfray, P., O'Doherty, S., Spain, T. G., and Jennings, G. S.: European greenhouse gas emissions estimated from continuous atmospheric measurements and radon 222 at Mace Head, Ireland, J. Geophys. Res., 105, 1351–1366, 2000. 8489

Chapman, S. and Cowling, T. G.: The Mathematical Theory of Non-Uniform Gases, Cambridge Univ. Press, Cambridge, 1970. 8475

Ciais, P., Denning, A. S., Tans, P. P., Berry, J. A., Randall, D. A., Collatz, G. J., Sellers, P. J., White, J. W. C., Trolier, M., Meijer, H. A. J., Francey, R. J., Monfray, P., and Heimann, M.: A three-dimensional synthesis study of $\delta^{18}O$ in atmospheric CO_2, 1. Surface fluxes, J. Geophys. Res., 102, 5857–5872, 1997a. 8475, 8484

Ciais, P., Tans, P. P., Denning, A. S., Francey, R. J., Trolier, M., Meijer, H. A. J., White, J. W. C., Berry, J. A., Randall, D. A., Collatz, G. J., Sellers, P. J., Monfray, P., and Heimann, M.: A three-dimensional synthesis study of $\delta^{18}O$ in atmospheric CO_2, 2. Simulations with the TM2 transport model, J. Geophys. Res., 102, 5873–5883, 1997b. 8484

Dongmann, G.: The contribution of land photosynthesis to the stationary enrichment of ^{18}O in the atmosphere, Radiat. Environ. Biophys., 11, 219–225, 1974. 8487

Dongmann, G., Nürnberg, H. W., Förstel, H., and Wagner, K.: On the enrichment of $H_2^{18}O$ in the leaves of transpiring plants, Radiat. Environ. Biophys., 11, 41–52, 1974. 8484

Dörr, H. and Münnich, K. O.: ^{222}Rn flux and soil air concentration profiles in West-Germany. Soil ^{222}Rn as tracer for gas transport in the unsaturated soil zone, Tellus, 42B, 20–28, 1990. 8489

Farquhar, G. D., Lloyd, J., Taylor, J. A., Flanagnan, L. B., Syvertsen, J. P., Hubick, K. T., Wong, S. C., and Ehleringer, J. R.: Vegetation effects on the isotope composition of oxygen in atmospheric CO_2, Nature, 363, 439–443, 1993. 8487

Friedli, H., Siegenthaler, U., Rauber, D., and Oeschger, H.: Measurements of concentration, $^{13}C/^{12}C$ and $^{18}O/^{16}O$ ratios of tropospheric carbon dioxide over Switzerland, Tellus, 39B, 80–88, 1987. 8475

Fuller, W. A.: Measurement Error Models, Wiley Series in Probability and Statistics, John Wiley & Sons, New York, 1987. 8481

Gemery, P. A., Trolier, M., and White, J. W. C.: Oxygen isotope exchange between carbon dioxide and water following atmospheric sampling using glass flasks, J. Geophys. Res., 101, 14 415–14 420, 1996. 8478

Grew, K. E. and Ibbs, T. L.: Thermal Diffusion in Gases, Cambridge Univ. Press, Cambridge, 1952. 8480

Guy, R. D., Fogel, M. L., and Berry, J. A.: Photosynthetic Fractionation of the Stable Isotopes of Oxygen and Carbon, Plant Physiol., 101, 37–47, 1993. 8487

Hesterberg, R.: Das Kohlendioxid und seine stabilen Isotope in Atmosphäre und Boden, Master's thesis, Physics Institute, University of Bern, Bern, Switzerland, 1990. 8475, 8495

Keeling, C. D.: The concentration and isotopic abundances of atmospheric carbon dioxide in rural areas, Geochim. Cosmochim. Acta, 13, 322–334, 1958. 8483
Keeling, C. D.: The concentration and isotopic abundances of carbon dioxide in rural and marine air, Geochim. Cosmochim. Acta, 24, 277–298, 1961. 8483
Keeling, C. D., Bacastow, R. B., Carter, A. F., Piper, S. C., Whorf, T. P., Heimann, M., Mook, W. G., and Roeloffzen, H.: A three-dimensional model of atmospheric CO_2 transport based on observed winds: 1. Analysis of observational data, in: Aspects of Climate Variability in the Pacific and the Western Americas, edited by: Peterson, D. H., Geophys. Monogr. Ser., 55, 165–236, AGU, Washington D.C., 1989. 8475
Keeling, R.: The atmospheric oxygen cycle: The oxygen isotopes of atmospheric CO_2 and O_2 and the O_2/N_2 ratio, Rev. Geophys., Supplement, 1253–1262, 1995. 8484
Keeling, R. F., Stephens, B. B., Najjar, R. G., Doney, S. C., Archer, D., and Heimann, M.: Seasonal variations in the atmospheric O_2/N_2 ratio in relation to the kinetics of air-sea gas exchange, Global Biogeochem. Cycles, 12, 141–163, 1998. 8475
Keeling, R. F., Blaine, T., Paplawsky, B., Katz, L., Atwood, C., and Brockwell, T.: Measurement of changes in atmospheric Ar/N_2 ratio using a rapid-switching, single-capillary mass spectrometer system, Tellus, 56B, 322–338, 2004. 8479, 8480
Kroopnick, P. and Craig, H.: Atmospheric Oxygen: Isotopic Composition and Solubility Fractionation, Science, 175, 54–55, 1972. 8484, 8487
Lang, C.: Bestimmung und Interpretation der Isotopen- und Elementverhältnisse von Luft aus polaren und alpinen Eisbohrkernen, insbesondere zur Temperaturrekonstruktion unter Ausnutzung des Effekts der Thermodiffusion, PhD thesis, Physics Institute, University of Bern, Bern, Switzerland, 1999. 8481
Langenfelds, R. L.: Studies of the global carbon cycle using atmospheric oxygen and associated tracers, PhD thesis, Univ. of Tasmania, Hobart, Tasmania, Australia, 2002. 8475
Lehmann, B. E., Ihly, B., Salzmann, S., Conen, F., and Simon, E.: An automatic static chamber for continuous ^{220}Rn and ^{222}Rn flux measurements from soil, Radiation Measurements, 38, 43–50, 2004. 8478
Leuenberger, M., Nyfeler, P., Moret, H. P., Sturm, P., and Huber, C.: A new gas inlet system for an isotope ratio mass spectrometer improves reproducibility, Rapid Commun. Mass Spectrom., 14, 1543–1551, 2000. 8478
Leuenberger, M., Eyer, M., Nyfeler, P., Stauffer, B., and Stocker, T. F.: High-resolution δ^{13}C measurements on ancient air extracted from less than 10 cm^3 of ice, Tellus, 55B, 138–144,

2003. 8477
Manning, A. C.: Temporal variability of atmospheric oxygen from both continuous measurements and a flask sampling network: Tools for studying the global carbon cycle, PhD thesis, University of California, San Diego, California, USA, 2001. 8475, 8481, 8485
Meijer, H. A. J., Neubert, R. E. M., and Visser, G. H.: Cross contamination in dual inlet isotope ratio mass spectrometers, International Journal of Mass Spectrometry, 198, 45–61, 2000. 8486
Pataki, D. E., Bowling, D. R., and Ehleringer, J. R.: Seasonal cycle of carbon dioxide and its isotopic composition in an urban atmosphere: Anthropogenic and biogenic effects, J. Geophys. Res., 108(D23), 4735, doi:10.1029/2003JD003865, 2003. 8484
Schmidt, M., Graul, R., Sartorius, H., and Levin, I.: Carbon dioxide and methane in continental Europe: a climatology, and ^{222}Radon-based emission estimates, Tellus, 48B, 457–473, 1996. 8488, 8489
Schmidt, M., Glatzel-Mattheier, H., Sartorius, H., Worthy, D. E., and Levin, I.: Western European N_2O emissions: A top-down approach based on atmospheric observations, J. Geophys. Res., 106, 5507–5516, 2001. 8488, 8489
Severinghaus, J. P.: Studies of the terrestrial O_2 and carbon cycles in sand dune gases and in Biosphere 2, PhD thesis, Columbia University, New York, USA, 1995. 8485
Severinghaus, J. P., Bender, M. L., Keeling, R. F., and Broecker, W. S.: Fractionation of soil gases by diffusion of water vapor, gravitational settling, and thermal diffusion, Geochim. Cosmochim. Acta, 60, 1005–1018, 1996. 8475
Stephens, B., Bakwin, P., Tans, P., and Teclaw, R.: Measurements of atmospheric O_2 variations at the WLEF tall-tower site, in Sixth International Carbon Dioxide Conference, Extended Abstracts, vol. I, pp. 78–80, Tohoku Univ., Sendai, Japan, 2001. 8486
Sturm, P.: Entwicklung eines neuen Einlasssystems für die massenspektrometrische Messung des O_2/N_2 Verhältnisses, Master's thesis, Physics Institute, University of Bern, Bern, Switzerland, 2001. 8478
Sturm, P., Leuenberger, M., Sirignano, C., Neubert, R. E. M., Meijer, H. A. J., Langenfelds, R., Brand, W. A., and Tohjima, Y.: Permeation of atmospheric gases through polymer O-rings used in flasks for air sampling, J. Geophys. Res., 109, D04309, doi:10.1029/2003JD004073, 2004. 8475, 8478
Sturm, P., Leuenberger, M., Moncrieff, J., and Ramonet, M.: Atmospheric O_2, CO_2 and $\delta^{13}C$ measurements from aircraft sampling over Griffin Forest, Perthshire, UK, Rapid Commun.

Mass Spectrom., 19, 2399–2406, DOI:10.1002/rcm.2071, 2005a. 8478, 8486
Sturm, P., Leuenberger, M., and Schmidt, M.: Atmospheric O_2, CO_2 and $\delta^{13}C$ observations from the remote sites Jungfraujoch, Switzerland, and Puy de Dôme, France, Geophys. Res. Lett., in press, 2005b. 8478, 8482
Wilkening, M. H. and Clements, W. E.: Radon 222 From the Ocean Surface, J. Geophys. Res., 80, 3828–3830, 1975. 8475

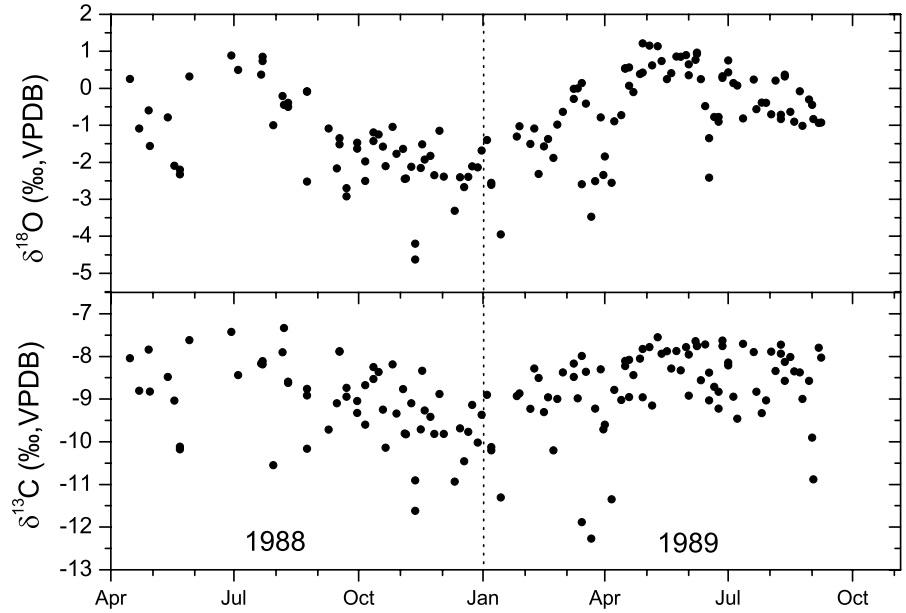

Fig. 1. $\delta^{13}C$ and $\delta^{18}O$ of CO_2 in Bern during a one-year period in 1988/89 (Hesterberg, 1990).

ACPD
5, 8473–8506, 2005

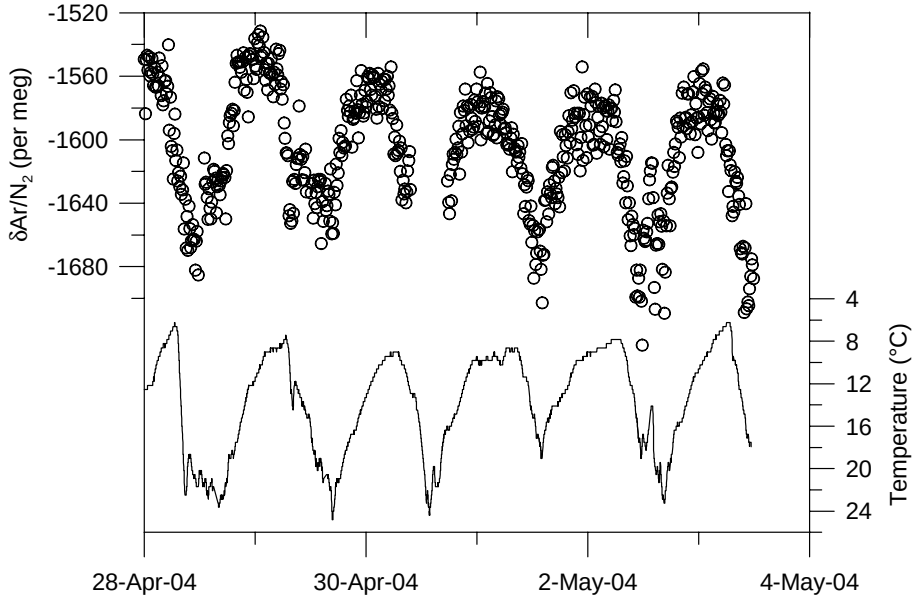

Fig. 2. Diurnal variations of $\delta Ar/N_2$ (top) and outdoor temperature (bottom). Note the inverted axis of the temperature.

ACPD

5, 8473–8506, 2005

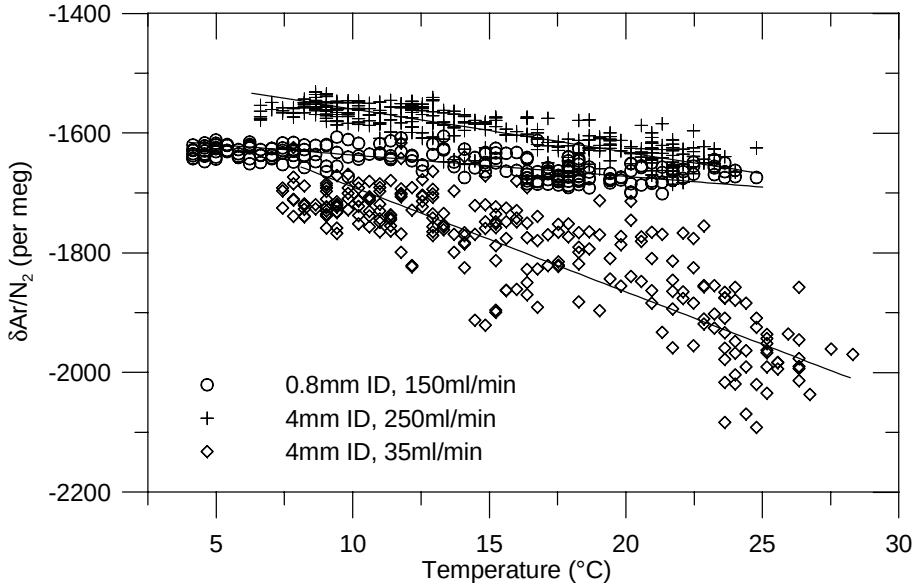

Fig. 3. Correlation of $\delta Ar/N_2$ and outdoor temperature for different types of air intake.

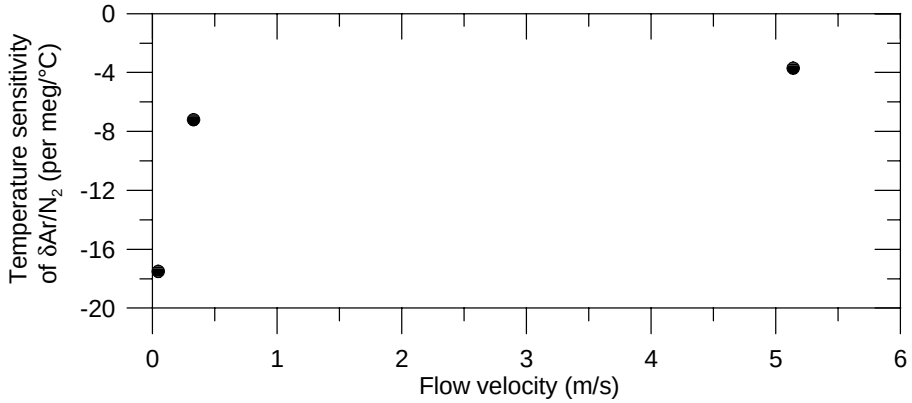

Fig. 4. Temperature sensitivity of $\delta \mathrm{Ar}/\mathrm{N}_2$ depending on the gas velocity at the air intake for the three experiments of Fig. 3.

ACPD
5, 8473–8506, 2005

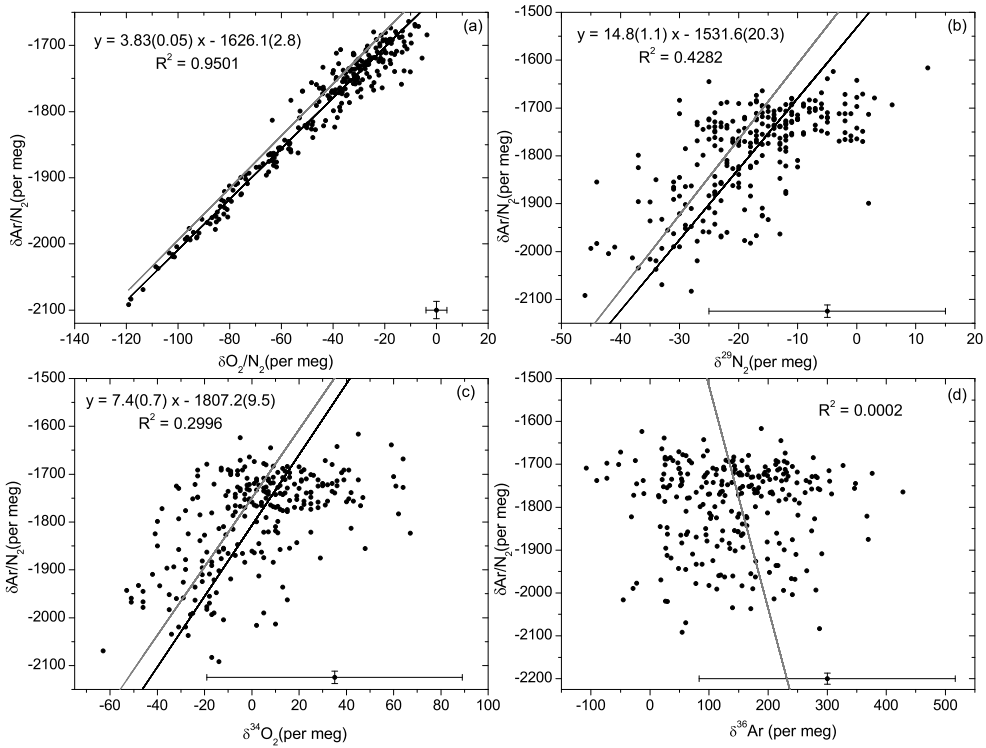

Fig. 5. Correlation plots of $\delta Ar/N_2$ versus O_2/N_2, $\delta^{29}N_2$, $\delta^{34}O_2$ and $\delta^{36}Ar$ for the "4 mm ID/35 mL min^{-1}" experiment (see text). Grey lines represent the expected correlation slopes obtained from the ratios of the thermal diffusion factors for the respective isotopes and elements. Black lines are the measured regression slopes using the associated errors as shown in the bottom part of each graph.

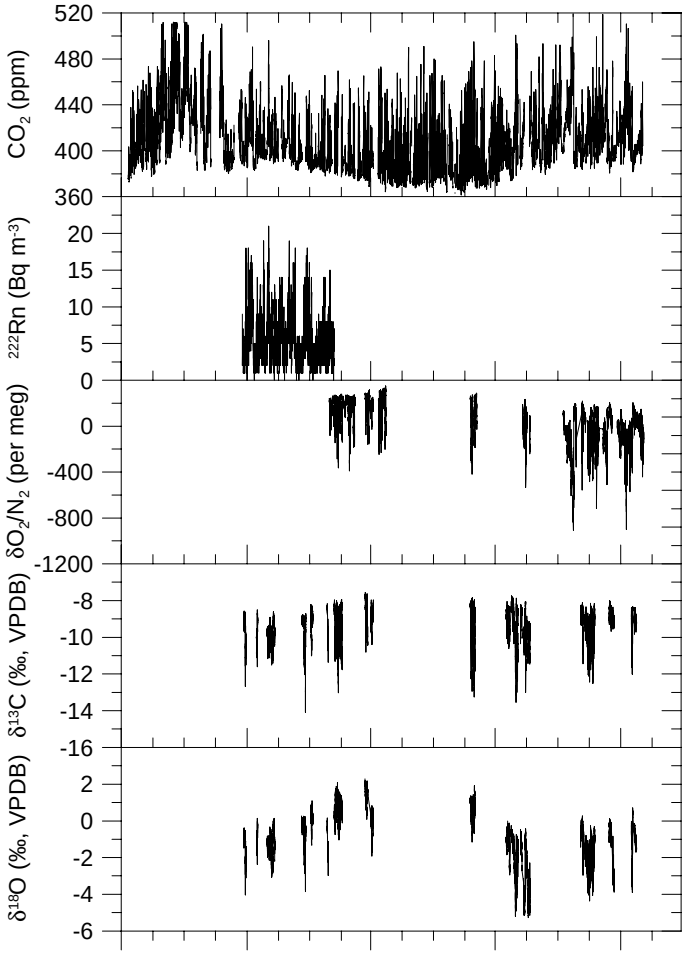

Fig. 6. Atmospheric records of CO_2, ^{222}Rn, O_2/N_2, $\delta^{13}C$ and $\delta^{18}O$ of CO_2 at Bern between October 2003 and February 2005.

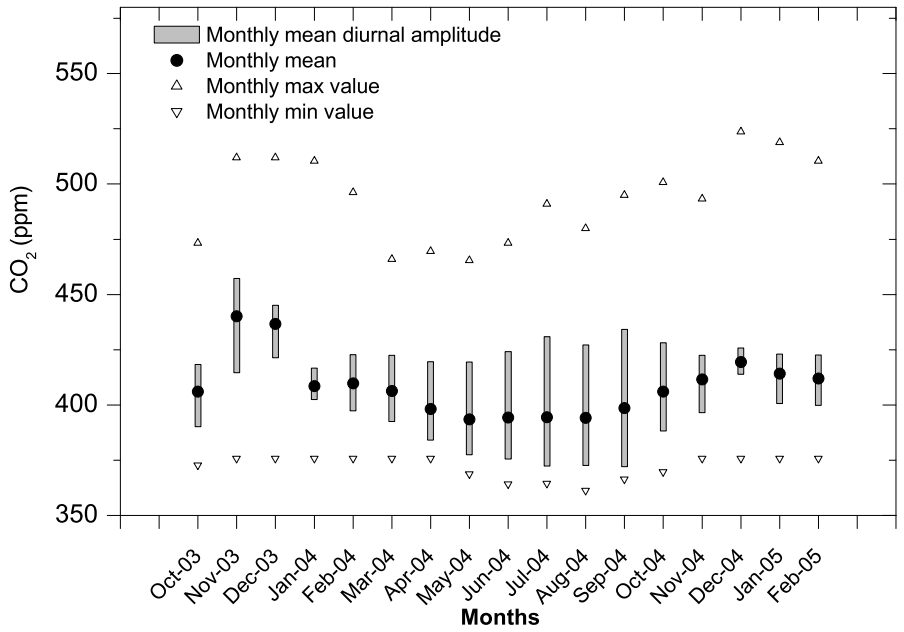

Fig. 7. Mean diurnal amplitudes (columns), monthly mean (black circles) and monthly maximum and minimum (triangles) of CO_2 for the months October 2003 to February 2005.

ACPD
5, 8473–8506, 2005

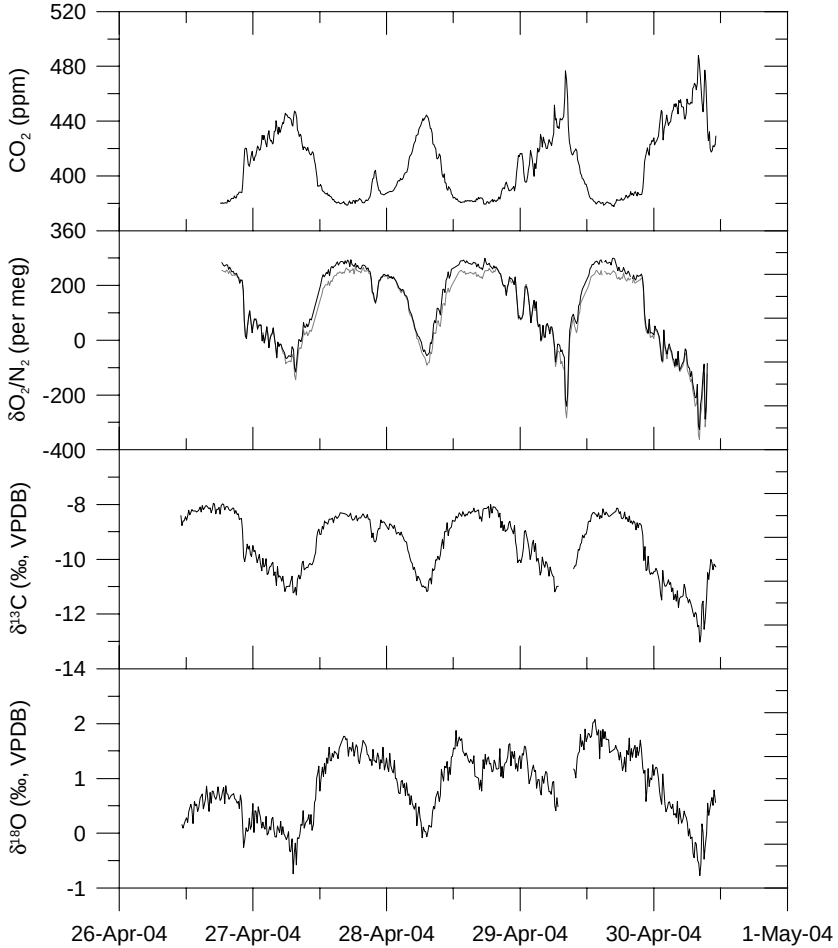

Fig. 8. Example of continuous CO_2, O_2/N_2, $\delta^{13}C$ and $\delta^{18}O$ records between 26 April and 1 May 2004. For the O_2/N_2 the original (shaded line) as well as the corrected values (black line) are shown (see text for explanation).

ACPD
5, 8473–8506, 2005

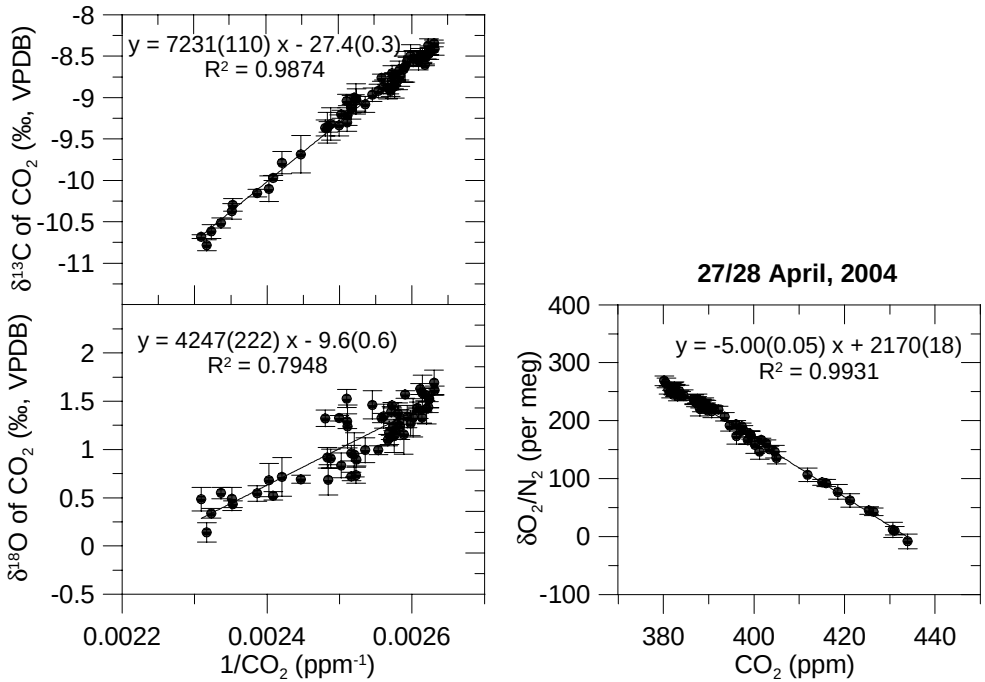

Fig. 9. Representative Keeling plot of carbon and oxygen isotope ratios and O_2:CO_2 oxidation ratio during the night (18:00 to 06:00 LT) of 27/28 April 2004. The equations shown are derived from geometric mean regression (uncertainty in parentheses).

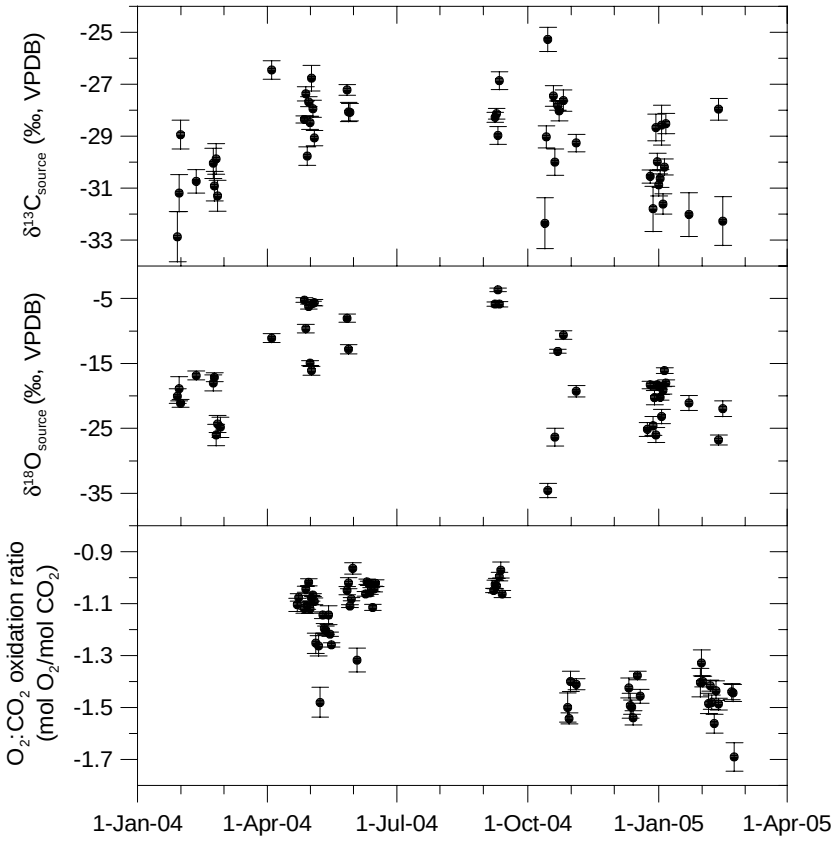

Fig. 10. $\delta^{13}C$ and $\delta^{18}O$ of source CO_2 calculated from Keeling plots, and O_2:CO_2 oxidation ratios.

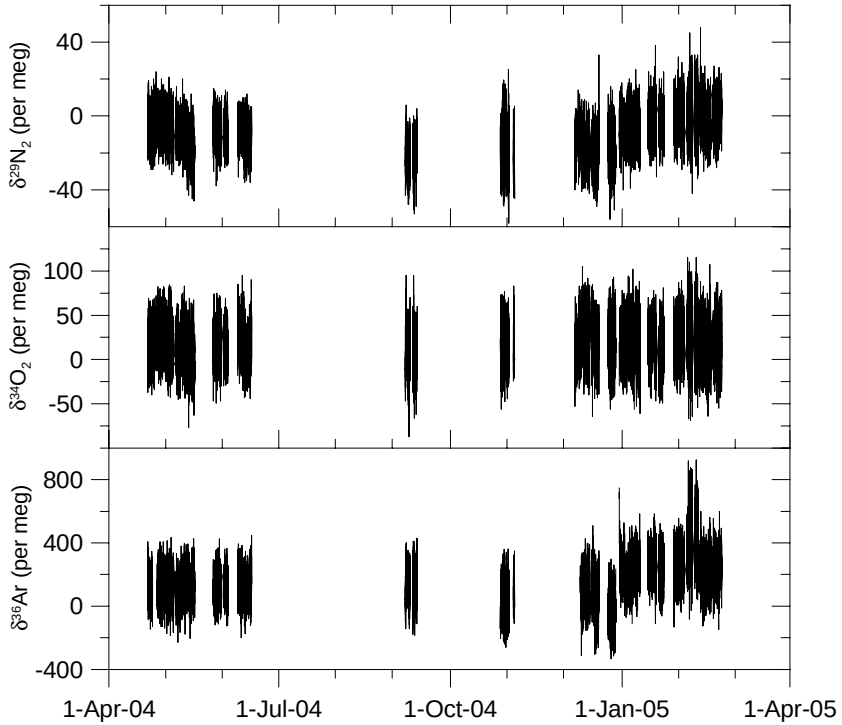

Fig. 11. Measurements of the isotopic ratios $\delta^{29}N_2$, $\delta^{34}O_2$ and $\delta^{36}Ar$ at Bern between April 2004 and February 2005.

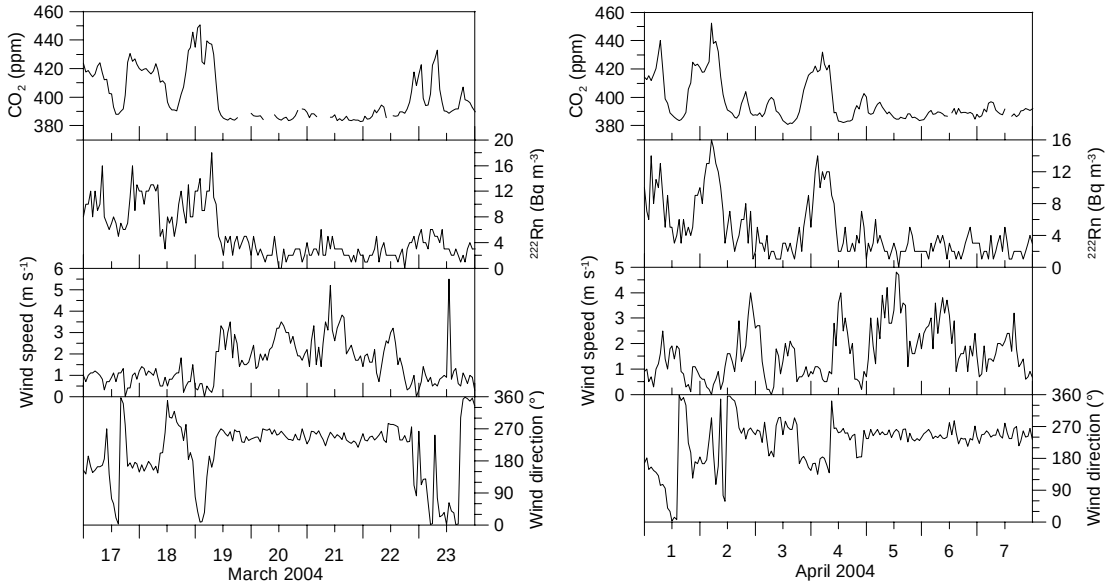

Fig. 12. Examples of hourly mean values of CO_2 and ^{222}Rn, together with local wind speed and wind direction between 17 and 23 March 2004 (left panel) and between 1 and 7 April 2004 (right panel).

ACPD
5, 8473–8506, 2005